Article

Ternary Holey Carbon Nanohorn/Potassium Chloride/Polyvinylpyrrolidone Nanohybrid as Sensing Film for Resistive Humidity Sensor

Bogdan-Catalin Serban [1,2], Octavian Buiu [1,2,*], Marius Bumbac [3,4,*], Nicolae Dumbravescu [1,2], Cristina Pachiu [1], Mihai Brezeanu [5], Gabriel Craciun [1], Cristina Mihaela Nicolescu [4], Vlad Diaconescu [6] and Cornel Cobianu [5,7]

[1] National Institute for Research and Development in Microtechnologies-IMT Bucharest, 126 A Erou Iancu Nicolae Str., 077190 Voluntari, Romania; bogdan.serban@imt.ro (B.-C.S.); nicolae.dumbravescu@imt.ro (N.D.); cristina.pachiu@imt.ro (C.P.); gabriel.craciun@imt.ro (G.C.)
[2] Research Center for Integrated Systems, Nanotechnologies, and Carbon-Based Nanomaterials (CENASIC)-I.M.T., 077190 Bucharest, Romania
[3] Sciences and Advanced Technologies Department, Faculty of Sciences and Arts, Valahia University of Targoviste, 13 Sinaia Alley, 130004 Targoviste, Romania
[4] Institute of Multidisciplinary Research for Science Technology, Valahia University of Targoviste, 13 Sinaia Alley, 130004 Targoviste, Romania; cristina.nicolescu@valahia.ro
[5] Department of Machines, Materials and Electric Drives, Faculty of Electrical Engineering, National University of Science and Technology Politehnica Bucharest, 313 Splaiul Independentei, 060042 Bucharest, Romania; scriemiceva@hotmail.com (M.B.); cornel.cobianu@upb.ro (C.C.)
[6] Faculty of Medicine, University of Medicine and Pharmacy "Carol Davila", Dionisie Lupu Street, No. 37, Sector 2, 030167 Bucharest, Romania; diaconescuvld506@gmail.com
[7] Academy of Romanian Scientists (A.R.S.), Str. Ilfov Nr. 3, Sector 5, 010071 Bucharest, Romania
* Correspondence: octavian.buiu@imt.ro (O.B.); marius.bumbac@valahia.ro (M.B.)

Abstract: The study presents findings on the relative humidity (R.H.) sensing capabilities of a resistive sensor. This sensor utilizes sensing layers composed of a ternary nanohybrid, consisting of holey carbon nanohorn (CNHox), potassium chloride (KCl), and polyvinylpyrrolidone (PVP), with mass ratios of 7/1/2, 6.5/1.5/2, and 6/2/2 (*w/w/w*). The sensing structure comprises a silicon substrate, a SiO_2 layer, and interdigitated transducer (IDT) electrodes. The sensing film is deposited on the sensing structure via the drop-casting method. The sensing layers' morphology and composition are investigated through Scanning Electron Microscopy (SEM) and RAMAN spectroscopy. The resistance of thin-film sensors based on ternary hybrids increased with exposure to a range of relative humidity (R.H.) levels, from 0% to 100%. The newly designed devices demonstrated a comparable response at room temperature to that of commercial capacitive R.H. sensors, boasting excellent linearity, swift response times, and heightened sensitivity. Notably, the studied sensors outperform others employing CNHox-based sensing layers in terms of sensitivity, as observed through manufacturing and testing processes. It elucidates the sensing mechanisms of each constituent within the ternary hybrid nanocomposites, delving into their chemical and physical properties, electronic characteristics, and affinity for water molecules. Various alternative sensing mechanisms are considered and discussed, including the reduction in holes within CNHox upon interaction with water molecules, proton conduction, and PVP swelling.

Keywords: holey carbon nanohorn (CNHox); potassium chloride (KCl); polyvinylpyrrolidone (PVP); nanohybrid; resistive R.H. sensor

1. Introduction

Humidity has become an essential environmental parameter in many residential, industrial, and commercial applications. Monitoring and controlling the humidity in offices, homes, and medical settings using gas supply infrastructure, respiratory care systems, incubators,

infusion pumps, ventilators, and sterilizers benefit human comfort. They measure humidity in the pharmaceutical industry (i.e., for packaging and storage), in the quality control of food and beverage production, and in the cosmetics industry. The control of humidity is essential in many industries, including electronics manufacturing (e.g., semiconductor production facilities), chemical processing (e.g., dehumidifiers, dryers), metallurgy, textiles, and papermaking. It is also important in agriculture (e.g., soil moisture detection), climatology, the automotive industry (e.g., engine test beds), and many others [1–5].

As a result, the humidity sensor market has experienced a significant growth over the past few decades and is projected to exceed USD 8.7 billion by 2029 [6,7]. Various types of humidity sensors are currently utilized across different applications. Among these, resistive R.H. sensors offer several advantages, including cost-effectiveness, simple design, a broad operating range, rapid response times, and low power consumption. However, they also have limitations such as lower accuracy and stability, non-linear response, and relatively shorter lifespan.

In addition to the sensing principle (electrochemical, optical, gravimetric, capacitive, piezoresistive, or resistive), fabrication techniques, and sensor design, the selection of materials for the sensing layer is crucial for developing humidity sensors with superior performance [8]. To date, numerous materials have been investigated for use as sensing layers in humidity sensor designs, as outlined in Table 1.

Table 1. Classification of sensing humidity materials based on sensitive response.

Type of Humidity Sensor	Sensitive Response	Reference
capacitive humidity sensors	the dielectric constant of the material changes, leading to a change in capacitance	polymers, carbon-based materials, metal oxide-based materials, composites, mesoporous silica, macroporous silica [9–11]
resistive humidity sensors	changes in the electrical resistance of the sensing material	polymers, carbon-based materials, metal oxide-based materials, composites, mesoporous silica [9,10,12]
thermal conductivity humidity sensors	thermal conductivity of air increases, leading to a change in temperature or heat flow within the sensor	polymers, ceramics, nanocomposites, carbon-based materials [13,14]
gravimetric humidity sensors	changes in mass or weight of a humidity-sensitive material	hygroscopic polymers or salts, porous materials, quartz crystal microbalance sensors [15]
optical humidity sensors	changes in optical properties, such as refractive index or absorbance	fiber optics coated with humidity-sensitive materials (photonic crystals, hygroscopic coatings, hydrogels, nanoparticles) [16]
surface acoustic wave (SAW) humidity sensors	the shift in frequency or phase of the acoustic waves on the surface of a piezoelectric substrate	polymers, carbon-based materials, metal oxide-based materials, composites [17]
electrolytic humidity sensors	the change of conductivity or impedance of the solution	hydrogel polymers, solid electrolytes, conductive polymer composites [18–21]

Furthermore, numerous carbon-based materials find widespread application as sensing layers in the construction of R.H. sensors. Their large specific surface area, capacity to function at room temperature, robust mechanical properties, notable chemical inertness,

and ease of hydrophilization through covalent functionalization render these materials particularly appealing as sensitive coatings for resistive humidity monitoring. Carbon nanofibers [22], carbon nanosheets [23], mesoporous carbon [24], amorphous carbon [25], carbon dots [26], N-doped hydrogenated amorphous carbon [27], nanodiamond [28], carbon nanocoil [29], carbon nanotubes and their nanocomposites [30,31], graphene oxide [32,33], reduced graphene oxide [34], fullerenol [35], and fullerenes [36] are some of the carbon nanomaterials studied for R.H. sensing applications.

In particular, thanks to their outstanding physical, chemical, and electrical properties, CNH-based materials have been widely used for R.H. sensing applications in the last few years. Several types of CNHs and their nanocomposites were used as sensing layers within the design of chemoresistive R.H. sensors: pristine C.N.H.s [37], oxidized carbon nanohorns (CNHoxs), binary nanocomposites, such as CNH-PVP, CNHox-PVP [38], and CNHox-poly(ethylene glycol)-block-poly(propylene glycol)-block-poly(ethylene glycol) [38], and ternary nanocomposites, such as GO-CNHox-PVP [39]. Furthermore, several mixtures, such as CNHox/SnO_2/ZnO/PVP [40], CNHox)/TiO_2/PVP [8], and CNHox/ZnO/PVP [41], were also used as sensing layers for R.H. resistive monitoring. Finally, alkali ions, such as K^+ [42–45], Li^+ [46,47], or Na^+ [48], were often used in fabricating R.H. sensors as dopants to improve their sensing parameters.

Several types of devices are available for R.H. monitoring, and these operate on a wide range of principles, such as capacitive [49], optical [50], surface acoustic wave [51], resistive [52], and electrochemical [53]. Resistive sensors have garnered heightened interest in recent decades owing to their straightforward design, cost-effectiveness, heightened sensitivity, and minimal energy usage. In this type of device, relative humidity (R.H.) measurement relies on the alteration in resistance within a humidity-sensitive layer upon interaction with water molecules in the gas phase. The introduction of water vapor triggers modifications in the resistance of the thin film through processes such as adsorption, absorption, swelling, and chemical reactions like dissociation and diffusion. These phenomena take place either on the surface or within the bulk of the thin film, serving as the sensing element [54,55].

This paper discusses the relative humidity (R.H.) sensing capabilities of a resistive sensor utilizing a sensing layer composed of a ternary nanohybrid containing CNHox/KCl/PVP at mass ratios of 7/1/2, 6.5/1.5/2, and 6/2/2 (*w/w/w*). The study highlights the R.H. sensing performance of the newly developed CNHox-based nanohybrid operating at room temperature (R.T.). Incorporating oxidized nanohorns with PVP and KCl aims to enhance sensitivity and selectivity in humidity sensing, addressing several research gaps and areas needing improvement in the field, such as sensitivity, response and recovery times, and sensor stability. The proposed mixture as a sensing substrate tackles these challenges by leveraging the unique properties of nanohorns, KCl, and PVP. Oxidized nanohorns are expected to boost the adsorption of water molecules, potentially broadening the sensors' sensitivity and dynamic range. Conversely, the combination of oxidized nanohorns with PVP and KCl may create a more accessible surface area for humidity interaction, thereby potentially accelerating the sensor's response to humidity changes. Additionally, the chemical stability of PVP, combined with the robust structural properties of nanohorns, could contribute to devices capable of maintaining performance over time and under varying environmental conditions.

2. Materials and Methods

2.1. Materials

All the materials utilized in the fabrication of the novel R.H. sensing layers were purchased from Sigma Aldrich (Redox Lab Supplies Com, Bucharest, Romania). The holey CNHox, depicted in Figure 1a, exhibits lengths ranging from 40 nm to 50 nm, diameters between 2 nm and 5 nm, and a specific surface area of approximately 1300–1400 m^2/g. As per the supplier, the CNHox employed in experiments is devoid of metal contamination, with graphite constituting the primary impurity at approximately 10%

(w/w). The structure of the employed PVP is depicted in Figure 1b and has an average molar weight of 40,000 g mol^{-1}. The KCl used in the experiments has 99.99% purity (with impurities $\leq$15.0 ppm in the trace metal analysis). Isopropyl alcohol ($(CH_3)_2CHOH$) is a 70% w/w solution in water. All reagents were used as-received without further purification.
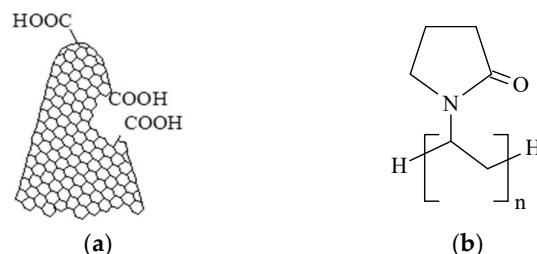

Figure 1. The structure of (**a**) holey CNHox and (**b**) PVP.

2.2. Preparation of the Quaternary Organic–Inorganic Holey CNH-Based Hybrid Sensing Films and Experimental Setup

To explore the relative humidity (R.H.) sensing performance of the ternary nanohybrid, sensing films with the following chemical compositions were formulated, prepared, and evaluated: CNHox/KCl/PVP ratios of 7/1/2, 6.5/1.5/2, and 6/2/2, all expressed as mass ratios ($w/w/w$). The mixture was homogenized in isopropyl alcohol using gentle sonication (FS20D Fisher Scientific, Dreieich, Germany), working at 42 kHz (output power of 70 W). This process provides a relatively uniform dispersion of the CNHox and KCl in the PVP network.

The preparation of sensing films based on CNHox, KCl, and PVP with varying weight ratios followed a five-step procedure. Initially, a PVP solution was prepared by dissolving 2 mg of the hydrophilic polymer in 10 mL of isopropyl alcohol and stirring it in an ultrasonic bath for 10 min. Subsequently, holey CNHox (7 mg, 6.5 mg, and 6 mg, respectively) was dispersed in the prepared PVP solution and stirred in the ultrasonic bath for 6 h at room temperature (R.T.). Following this, KCl powder was added to the resulting suspension to obtain the desired mass ratios (1 mg, 1.5 mg, and 2 mg of KCl), and continuous stirring was maintained in the ultrasound bath for another 6 h, also at R.T. Finally, the sensing layer was obtained using the drop-casting method, depositing the mixture onto the support structure. The electrical contact areas were masked before applying the sensing dispersion. All samples were then dried at 373 K for 60 min before conducting electrical measurements.

The sensing support structure consists of a metallic interdigitated electrode (IDE) with a dual-comb structure fabricated on a Si substrate (470 µm thickness), covered by a SiO$_2$ layer (1 µm thickness) (Figure 2). The IDE's metal stripes comprise chromium (10 nm thickness) and gold (100 nm thickness) [39–41,56].
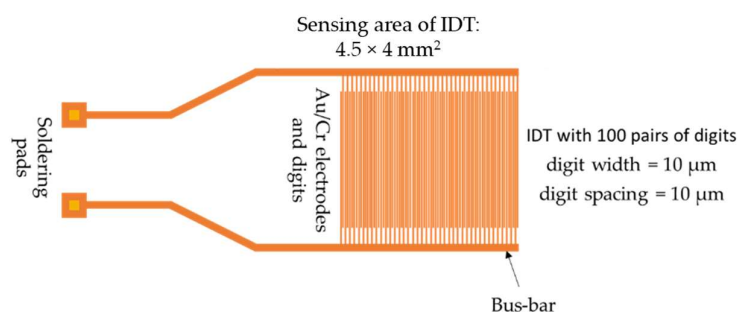

Figure 2. The layout of the IDE sensing structure.

The relative humidity (R.H.) monitoring experiments were conducted using a suitable experimental setup (see Figure 3). Dry nitrogen was introduced through a series of bubblers containing deionized water (conductivity below 1 µS/cm) to achieve controlled variations

in R.H. within the testing chamber, ranging from 0% to 100% R.H. The testing chamber accommodated two sensors: a commercial capacitive R.H. sensor (referred to as C.O.M.) as the reference and the new resistive sensing structure (abbreviated as S.U.I.—"sensor under investigation"). The sensing layers of the S.U.I. comprised nanocomposite mixtures of CNHox/KCl/PVP at various *w/w/w* ratios.
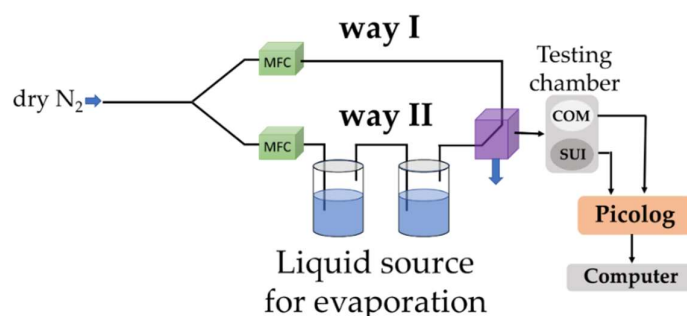

Figure 3. Experimental setup employed for R.H. measurements.

To figure out the function of individual components in the mixture, KCl added to the mix was chosen as the component for the study (concentrations of 10, 15, and 20%, while maintaining the PVP concentration constant).

The C.O.M. reference sensor confirmed the relative humidity (R.H.) level generated by controlling the mass flow controller and facilitated an objective comparison of the data measured by the S.U.I. Both sensors were positioned closely together and near the gas inlet to ensure exposure to identical gas flow and nearly identical experimental conditions. A Keithley 6620 current source (Keithley Instruments GmbH, Germering, Germany) supplied a direct current ranging from 0.01 to 0.1 A. Data acquisition and analysis were conducted using a PicoLog data logger (PICO Technology, Neots, Cambridgeshire, United Kingdom). All measurements were conducted at room temperature (R.T.).

The relative humidity (R.H.) sensing capabilities of each ternary nanohybrid-based sensing layer were investigated by applying a current across the two electrodes and recording the voltage difference while varying the R.H. from 0% to 100%. For simplicity in analysis, the following abbreviations are utilized:

Sensor K1: CNHox/KCl/PVP at a mass ratio of 7/1/2 (*w/w/w*).
Sensor K2: CNHox/KCl/PVP at a mass ratio of 6.5/1.5/2 (*w/w/w*).
Sensor K3: CNHox/KCl/PVP at a mass ratio of 6/2/2 (*w/w/w*).

Throughout the sensor realization process, particular attention was given to the potential variability induced by the processing steps. The IDT structures were achieved using a photolithographic process with practically zero-dimensional variations. The preparation of the sensing material included a homogenization step before the material was drop-cast on the IDTs. The process was implemented using between 25 and 30 different structures for each composition. After drying, the electrical resistance of each IDT structure was measured, and an average value (Rav) was determined; samples whose electrical resistance was outside the Rav ± 5% were excluded from the following steps (i.e., recording the electrical resistance vs. R.H. variations). For each group of samples (corresponding to different material compositions), the remaining samples were between 12 and 15. The results presented in the manuscript are typical results reflecting the behavior of the samples in each group.

The Raman spectra were acquired at room temperature (R.T.) using a Witec Raman spectrometer (Alpha-SNOM 300 S, WiTec. GmbH, Ulm, Germany) with 532 nm excitation. A 532 nm diode-pumped solid-state laser with 145 mW of power was employed. The incident laser beam, with a spot size of approximately 1.0 µm, was focused onto the sample using a 6 mm working distance objective attached to a Thorlabs MY100X-806 microscope. Raman spectra were recorded with an exposure time of 20 s accumulation, and the scattered light was collected by the same objective in back-scattering geometry with 600 grooves/mm

grating. The Raman systems underwent calibration using the 520 cm^{-1} Raman line of a silicon wafer. Data acquisition and processing were carried out by a dedicated computer using WiTec Project Five software (Version: 5.1).

Scanning electron microscopy (SEM) investigated the sensing films' surface topography. A field emission gun scanning electron microscope, FEG-SEM-Nova NanoSEM 630 (Thermo Scientific, Waltham, MA, USA) (F.E.I.), was used for surface visualization and had superior low-voltage resolution and high surface sensitivity imaging. The samples were investigated directly (i.e., no sample preparation was needed). The current during the measurements was 1 nA.

3. Results

3.1. Surface Topography

Scanning electron micrographs reveal that the surface morphology of the coating mixture appears relatively uniform across all cases (Figure 4a–f). Additionally, particles of significantly larger dimensions (>100 nm) are observable, attributed to the aggregation of particles with varied sizes and crystallographic orientations.
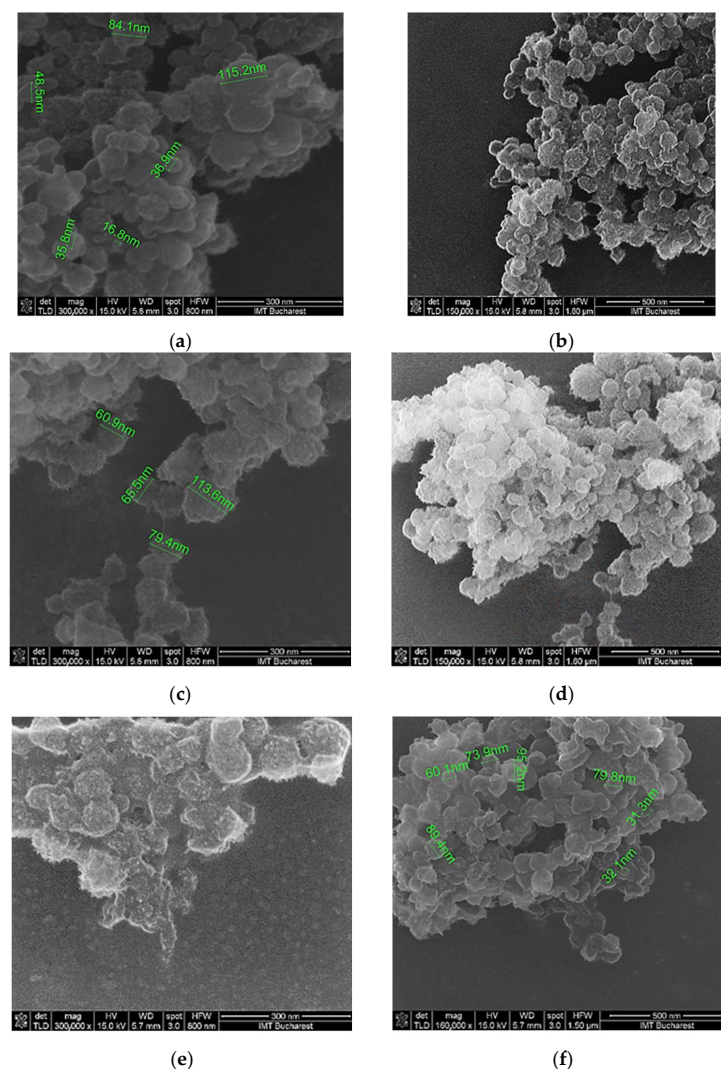

(a)   (b)

(c)   (d)

(e)   (f)

Figure 4. SEM of the K1' sensing layer at (**a**) ×300,000 magnification and (**b**) ×150,000 magnification, the K2' sensing layer at (**c**) ×300,000 magnification and (**d**) ×160,000 magnification, and the K3' sensing layer at (**e**) ×300,000 magnification and (**f**) ×160,000 magnification.

3.2. Raman Spectroscopy

The Raman spectra of the ternary nanohybrid CNHox/KCl/PVP are presented in Figure 5a,c. In Figure 5d, spectra p1–p3 are three acquisition points per sample (sample K3). In the p2 (gray) and p3 (black) spectra, between 0–1000 cm^{-1}, there are the vibration modes of Si combined with PVP; above 2700 cm^{-1}, there is a vibration mode specific to PVP (the Raman spectra of pure PVP is represented in blue). The Raman spectrum of powder PVP, for wavelengths below 1000 cm^{-1}, includes vibration lines associated with groups N-C=O (560 cm^{-1}) and C-C (758 cm^{-1}, 851 cm^{-1}, and 934 cm^{-1})
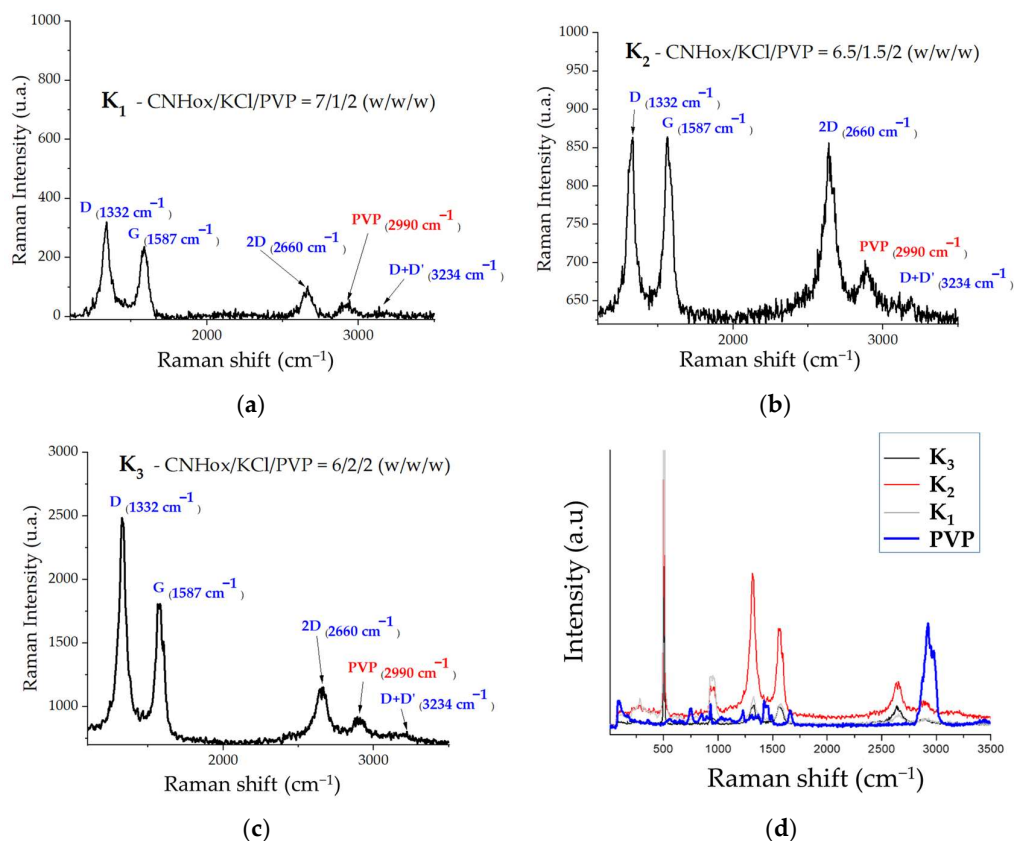

Figure 5. Raman spectra of ternary nanocomposite CNHox/KCl/PVP. (**a**) K1, (**b**) K2; (**c**) is K3; (**d**) three acquisition points of K3.

Three active Raman bands (D, G, 2D) were detected at wavenumbers of 1332, 1587, and 2660 cm^{-1}, respectively, which are characteristic of sp^2-defected carbon nanomaterials. Additionally, the Raman spectrum of pure PVP reveals a weak band at 2990 cm^{-1}, which can be attributed to PVP [57].

3.3. R.H. Monitoring Capability of the Ternary Nanocomposite

The present R.T. resistive R.H. sensor has an organic–inorganic sensitive layer containing oxidated carbon nanohorn (CNHox) with a concentration higher than the percolation threshold of the solid-state nanocomposite (Serban, B.-C., et al., 2021). This chemical design of the nanocarbon component assured a reasonably low value of the electrical conductivity of the sensing layer and simple, functional device measurability.

Figure 6 illustrates the relative humidity (R.H.) response of the fabricated sensors. It is evident that the resistance of the thin film based on the ternary nanohybrid increases with the rising of R.H.
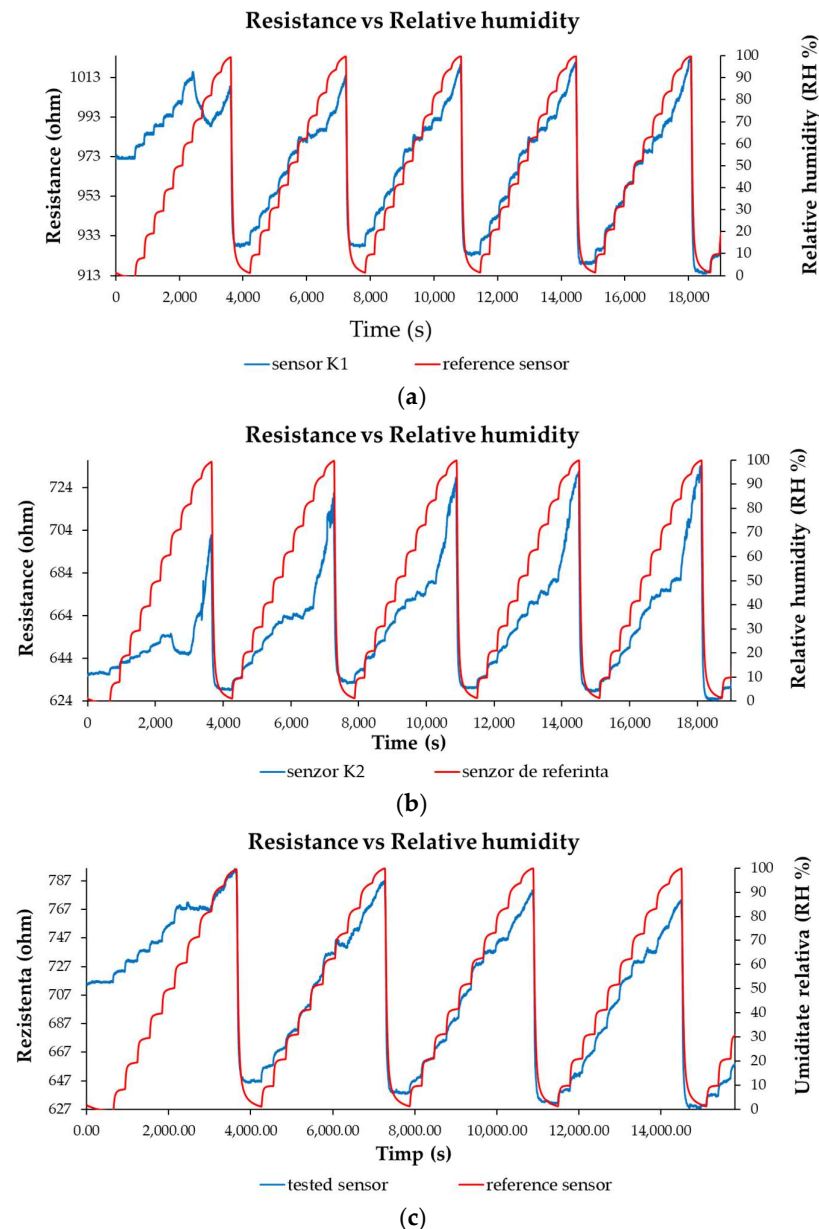
Figure 6. Resistance versus R.H. for the (**a**) K1, (**b**) K2, and (**c**) K3 sensors in several operating sequences.

At the same time, the overall linearity of the ternary nanohybrid-based resistive sensors—in humid nitrogen, when varying R.H. from 0% to 100%—is excellent, as shown in Figure 7. In terms of linearity, all the manufactured sensors show superior performances ($R^2 > 0.99$) for operating cycles 2–6 and an excellent baseline drift, but for R.H. values up to 80%. It is interesting to note a different behavior in the first operating cycle compared to other operating cycles. At R.H. higher than 80%, a sharp increase in resistance with R.H. can be observed.

For all studied sensing layers, there is a decrease in thin-film resistance following the first operating cycle. This decrease is more pronounced in sensors with higher KCl concentrations in the sensing layer. The results of this experiment reinforce the hypothesis that ionic conduction is the primary mechanism during the first operating cycle. Thus, adding potassium salt can provide more active sites for humidity, increasing the local concentration of water molecules in the sensing layer. Furthermore, the results presented in Figure 4 show a baseline drift for all tested sensing devices.
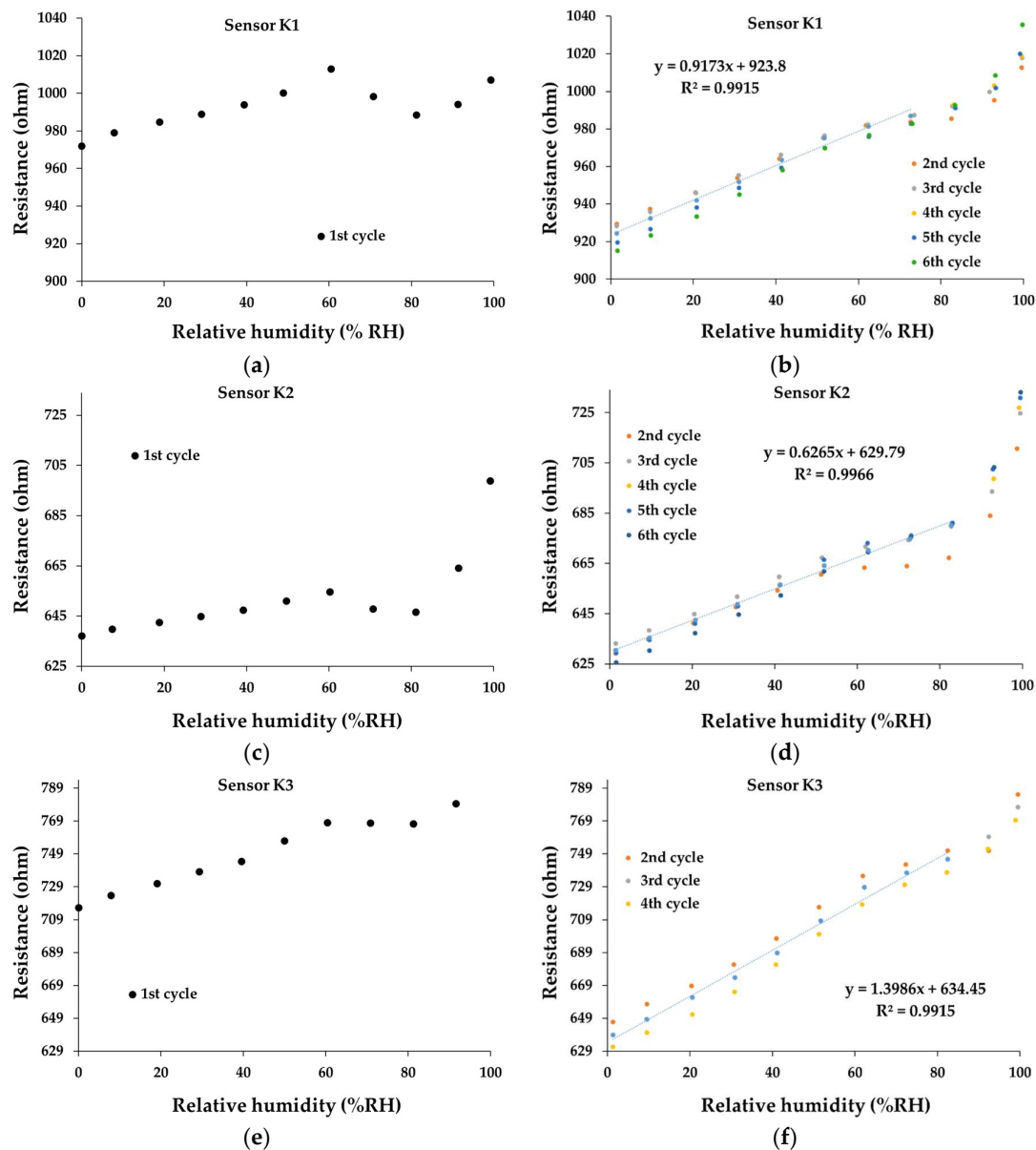
Figure 7. The transfer function of the sensor: (**a**) K1—1st cycle, (**b**) K1—2nd to 6th cycles, (**c**) K2—1st cycle, (**d**) K2—2nd to 6th cycles, (**e**) K3—1st cycle, and (**f**) K3—2nd to 6th cycles in humid nitrogen (R.H. = 0%–100%).

This study provides strong evidence that the presence of KCl significantly impacts the device's response during the first cycle. This influence is likely due to potassium ions bonding with water molecules, thereby changing material properties, particularly the electrical conductivity, which is further reflected in the electrical resistance change. This initial absorption phenomenon offers a potential explanation for the observed baseline drift in the first cycle.

Our experimental findings suggest that the sensor's initial exposure to moisture acts as a conditioning phase. During this phase, the sensor's sensing material undergoes physical or chemical changes that stabilize its response in subsequent humidity cycles. These changes might include the swelling of the polymer matrix, the redistribution of potassium chloride (KCl) and nanohorns within the composite material, or the alterations in the material's microstructure that affect its response to humidity.

After the initial cycle, the material might reach a state of equilibrium faster in subsequent cycles, showing less deviation in resistance measurements. This stabilization

could suggest that the initial drift is a part of a necessary "settling" process for the sensor materials.

The drop in resistance at higher relative humidity levels is related to the KCl content in the mixture. The evolution of resistance presented in Figure 6 shows that the sensing device of the K1 device is "settled" after a few functioning cycles. When the amount of KCl is increased, the device resistance increases upon exposure to a higher level of R.H. because more water molecules penetrate the bulk of the sensing layer. Therefore, KCl and water make a homogenous mixture in the sensing layer at higher water uptake. This could change the sensing structure response and possibly cause non-linear behavior at higher humidity levels, especially for the sensing coatings with increased KCl content.

Figure 7e,f present the transfer function for the sensor K3. Noticeably, after the first cycle, the resistance at R.H. = 0 reduces from 710–715 Ω to 630–635 Ω. The same behavior is also registered for the sensor K1 (Figure 7a,b), with a decrease in resistance (for R.H. = 0) from 970 (first cycle) to 910 Ω and 930 Ω (subsequent cycles).

The calculation of sensitivity was performed using the following equation:

$$S = \frac{\Delta R_x}{\Delta RH_x} = \frac{R_x - R_0}{RH_x}, \tag{1}$$

where Rx is the resistance of the sensitive layer measured in the test chamber for the [x–%] R.H. value indicated by the commercial sensor (measured with $\pm 2\%$ accuracy as the producer indicates it). R_0 is the value of resistance calculated from the linear function established from the graph of resistance and is equal to f (relative humidity) obtained by extrapolation for the value at 0% R.H. The calculated relative sensitivity values for each humidity jump are presented in Figure 8a–c.
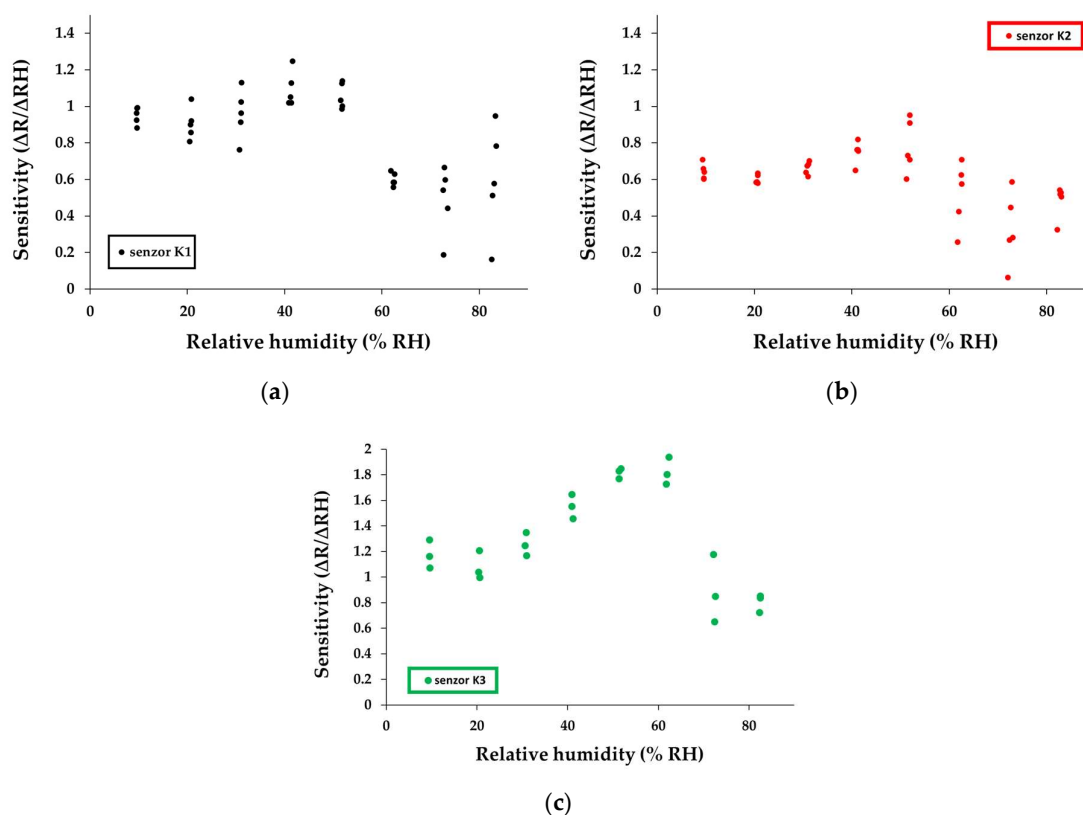

Figure 8. Sensitivity calculated for each humidity jump for sensors: (**a**) K1, (**b**) K2, and (**c**) K3 in humid nitrogen (R.H. = 0%–90%).

A simple comparison between the calculated sensitivities for K1, K2, and K3 sensors and other similarly manufactured and tested sensors that employed holey CNHOx–based

sensing layers reveals interesting results (Table 2). As one can see, K1, K2, and K3 sensors exhibit a superior performance in terms of sensitivity compared with other reported sensors. The high hydrophilicity of the alkali salt has a significant contribution, increasing the number of active sites towards water molecules. In addition, the enhanced sensing layer porosity and its associated high specific surface area can also contribute to this result.

Table 2. Comparison between different CNHox-based R.H. sensing layers and sensing performances for similarly manufactured and tested sensors.

Sensing Layer (Mass Ratio)	Sensitivity (S = $\frac{\Delta R}{\Delta RH}$) ($\Omega$/%R.H.)	Reference
CNHox	0.013–0.021	[35]
CNHox/PVP 1/1	0.020–0.058	[38]
CNHox/PVP 1/2	0.017–0.025	[38]
CNHox/GO/PVP 3/1/1	0,043–0, 051	[38]
CNHox/GO/SnO$_2$/PVP 0.75/0.75/1/1	0.548–0.770	[56]
CNHox/G.O./SnO$_2$/PVP 1/1/1/1	0.798–0.980	[56]
CNHox/KCl/PVP 7/1/2 (K1)	0.200–1.245	This work
CNHox/KCl/PVP 6.5/1.5/2 (K2)	0.300–0.950	This work
CNHox/KCl/PVP 6/2/2 (K3)	0.650–1.940	This work

An important parameter, such as response time (t_r), was calculated for all manufactured R.H. resistive sensors. If R(t) is the response of the device in time, t_r can be calculated as follows:

$$t_r = t_{90} - t_{10} \tag{2}$$

where t_{90} and t_{10} represent the moments when the response R(t) reaches 90% and 10%, respectively, from the total variation of the sensor's resistance due to a change in the R.H. value (as in the example presented in Figure 9).
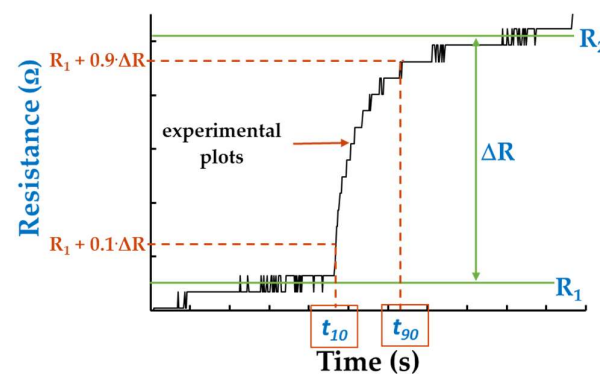

Figure 9. Example of calculating the response time.

Figure 10 presents the graphical representations of the investigated sensor's response time ratios relative to the reference sensor's (C.O.M.) response time calculated for each R.H. jump in humid nitrogen (R.H. = 0%–100%).
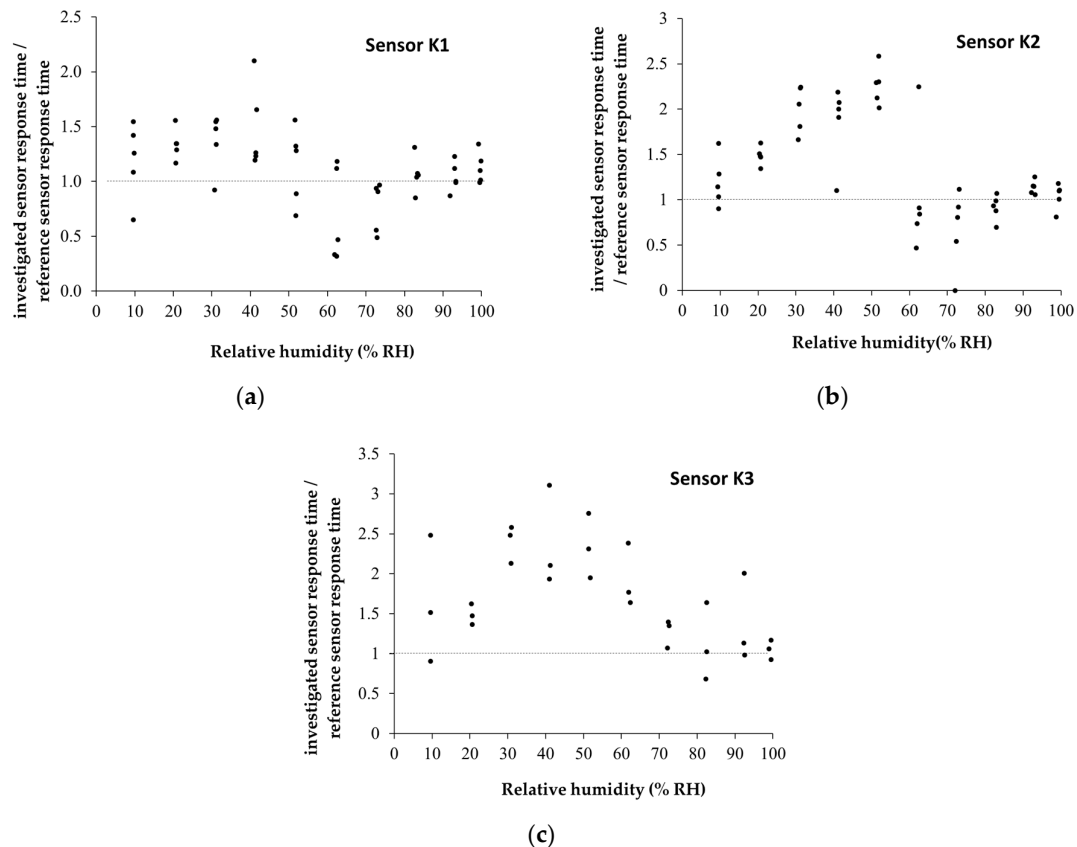
Figure 10. Graphical representations of the ratios between the response time of investigated sensors and the response time of C.O.M. calculated for each humidity jump: (**a**) K1, (**b**) K2, and (**c**) K3 in humid nitrogen (R.H. = 0%–100%).

The reference sensor has a response time of 60 s +/− 10 s for R.H. below 70%. The response time for R.H. > 70% increases to approximately 90 s +/−10 s. Water molecules permeate the hydrophilic nanohybrid sensing film. The hybrid nanocomposite film adsorbs/absorbs a substantial amount of water (related to the sensing film's mass). Finally, some water molecules can condense in the proximity of hydrophilic groups, thus blocking the active sites.

4. Analysis of the Sensing Mechanism

All constituents of the ternary nanohybrid used as a sensing layer in the resistive monitoring of R.H. have some outstanding chemical and physical properties. CNHox shows increased conductivity (p-type semiconductor behavior), a remarkable and controllable surface area (1300 to 1400 m^2/g), high porosity, hydrophilicity, and a rapid variation in the electrical resistance in contact with a water molecule in the 0% R.H. to 100% R.H. range. Furthermore, low-cost synthesis of CNHox via oxygen plasma treatment of the pristine carbon nanohorns (CNHs) is a simple, clean, and fast procedure. Finally, the functionalization of the CNHs in oxygen plasma has the advantage (by varying the exposure time and its power) that it can provide an optimal C:O ratio for superior sensitivity towards water molecules [58].

At the same time, PVP is a hydrophilic polymer with excellent binding and dispersion properties. The addition of alkali ions, such as K$^+$, ensures more active sites for water molecules.

The humidity-sensing film operates through three distinct mechanisms, considering the properties of its constituents. First, we analyze the p-type semiconducting behavior of the CNHox material. When exposed to water molecules, the CNHox accepts electron pairs, reducing the number of positive charge carriers (holes) within the nanocarbon material.

Consequently, the humidity-sensing film becomes more resistive. Several reviews reported in the literature confirm this interpretation [59].

The second sensing mechanism considers the dissociation of water. Due to the strong electrostatic field and high local charge density, the adsorbed water molecules on the CNHox hydrophilic surface and mesopores may dissociate into H^+ and OH^- ions. The protons generated by the water dissociation process may tunnel from one water molecule to another through hydrogen bonding, thus increasing the overall electrical conductivity of the sensitive film [60].

PVP is a dielectric polymer with hydrophilic properties, which swells after interaction with water molecules and has a negligible change in resistance in response to R.H. variation, as shown in literature for the presented composites [61–63]. Based on these properties, a third sensing mechanism can be discussed. The swelling of PVP leads to the displacement of CNHox, increases the distance between nanocarbon particles, and lowers the number of electrically percolating pathways. Accordingly, the device resistance increases upon exposure to a higher level of R.H. because more water molecules penetrate the bulk of the sensing layer.

Finally, the contribution of KCl to the sensing mechanism can be interpreted from two perspectives. Firstly, according to the Hard–Soft Acid–Base (HSAB) theory, the K+ ion is classified as a hard acid and can electrostatically interact with water molecules, which are classified as hard bases (electron donors) [64,65]. Thus, adding potassium salt can provide more active sites for humidity, increasing the local concentration of water molecules in the sensing layer. Due to the p-type semiconducting behavior of CNHox and the PVP swelling, a higher number of water molecules leads to a significant increase in resistance. At the same time, once the local concentration of water molecules increases, KCl is dissolved, the ions can move freely, and the conductivity of the sensing layer increases.

In conclusion, as described above, the interaction of the sensing layer with water molecules has, theoretically, antagonistic effects on its resistance variation. Since the measured resistance of the sensing film increases when R.H. increases from 0% to 100%, one can assume that the cumulative effect of the p-type semiconductor behavior of the CNHox and the swelling of PVP are the dominant causes that lead to this effect. Therefore, without completely excluding the impact of both the proton-tunneling mechanism and ionic conduction through K+ and Cl- ions, the interaction of the CNHox-PVP tandem with water has a pivotal contribution to the variation in the resistance of the sensing layer with R.H.

For all studied sensing layers, the thin film's resistance decreases after the sensor's first operating cycle. The higher the percentage of KCl in the sensitive layer, the more significant the decrease in resistance. This experimental result agrees with the idea that the ionic conduction mechanism is predominant in the first operating cycle.

5. Conclusions

The proposed study investigated the relative humidity (R.H.) sensing response of an R.H. detection structure employing a ternary nanohybrid as a sensing layer. The nanohybrid consisted of holey CNHox (with concentration levels surpassing the percolation threshold), KCl, and PVP, with mass ratios of 7/1/2, 6.5/1.5/2, and 6/2/2 (*w/w/w*). The sensing structure comprised a silicon substrate, a SiO_2 layer, and an interdigitated electrode (IDE). The sensing film was deposited onto the sensing structure using the drop-casting method. The morphology and composition of the sensing layers were investigated using scanning electron microscopy (SEM) and Raman spectroscopy.

The manufactured sensors exhibited a favorable room temperature response comparable to that of a commercial capacitive R.H. sensor. They demonstrated excellent linearity, rapid response times, and good sensitivity. Moreover, they showed superior sensitivity performance compared to other sensors employing holey CNHox-based sensing layers. Regarding linearity, all manufactured sensors demonstrated superior performance (R2 > 0.99) for operating cycles 2–6 and exhibited minimal baseline drift up to an R.H. of

80%. However, at R.H. levels exceeding 80%, increased water molecule permeation into the hydrophilic nanohybrid sensing film was observed. The hybrid nanocomposite film absorbed a significant amount of water, proportional to the sensing film's mass. Eventually, some water molecules condensed near the hydrophilic groups, potentially obstructing active sites. Although the K3 sensor shows a more significant variation in resistance when humidity varies between 0 and 100% R.H. (about 170 ohms between the minimum and maximum resistance values measured during the experiment), its response is not linear when humidity exceeds 60% R.H. The same phenomenon was recorded for the K2 sensing device. Therefore, the K1 sensor has the closest response to the reference sensor, presenting at the same time a resistance variation of approximately 130 ohms, which could allow its use for devices with high sensitivity for relative humidity measurement.

The role of each component in the ternary nanohybrid used as a sensing film was thoroughly explained, considering their electrical, chemical, and physical properties. Three distinct sensing mechanisms were explored and discussed. Notably, the p-type semiconductor behavior of CNHox, combined with the swelling of the hydrophilic polymer (PVP), was found to dominate. As a result, the overall resistance of the sensing films increased with relative humidity (R.H.) across all manufactured sensors.

The significant advantages of the presented sensors include their low power consumption, which is below 2 mW, their reliable sensing performance at room temperature, and their straightforward manufacturing process. The evaluated sensing coatings demonstrate exceptional performance for atmospheric sensors, facilitating tasks such as environmental monitoring, indoor air quality assessment, and industrial processes. These coatings deliver precise measurement accuracy within relative humidity (R.H.) ranges up to 80%. Interestingly, the decrease in resistance beyond 80% humidity can be utilized as a valuable feature rather than a drawback. This characteristic enables the triggering of alarm signals or the activation of control systems in critical applications. Such applications include electronic equipment rooms, storage facilities, sensitive manufacturing areas, chemical processing plants, laboratories handling moisture-sensitive materials, and battery energy storage facilities, where maintaining humidity below a specific threshold is crucial.

6. Patents

Bogdan-Catalin Serban, Octavian Buiu, Marius Bumbac, Cristina Mihaela Nicolescu, Nanohibrid ternar pentru monitorizarea rezistiva a umiditatii relative, Romanian patent application, the official bulletin of industrial property, OSIM, 137854A2, 29 December 2023.

Institutional Review Board Statement: Not applicable.

Informed Consent Statement: Not applicable.

Data Availability Statement: Data are contained within the article.

Conflicts of Interest: The authors declare no conflicts of interest.

References

1. Ma, Z.; Fei, T.; Zhang, T. An overview: Sensors for low humidity detection. *Sens. Actuators B Chem.* **2023**, *376*, 133039. [CrossRef]
2. Ku, C.A.; Chung, C.K. Advances in Humidity Nanosensors and Their Application. *Sensors* **2023**, *23*, 2328. [CrossRef] [PubMed]
3. Huang, C.; Jiang, M.; Liu, F. Recent Progress on Environmentally Friendly Humidity Sensor: A Mini Review. *ACS Appl. Electron. Mater.* **2023**, *5*, 4067–4079. [CrossRef]
4. Farhan, K.Z.; Shihata, A.S.; Anwar, M.I.; Demirboğa, R. Temperature and humidity sensor technology for concrete health assessment: A review. *Innov. Infrastruct. Solut.* **2023**, *8*, 276. [CrossRef]
5. Kumar, A.; Gupta, G.; Bapna, K.; Shivagan, D.D. Semiconductor-metal-oxide-based nanocomposites for humidity sensing applications. *Mater. Res. Bull.* **2023**, *158*, 112053. [CrossRef]
6. Barmpakos, D.; Kaltsas, G. A review on humidity, temperature and strain printed sensors—Current trends and future perspectives. *Sensors* **2021**, *21*, 739. [CrossRef]
7. Global Humidity Sensor Market—Industry Trends and Forecast to 2029. Available online: https://www.databridgemarketresearch.com/reports/global-humidity-sensor-market (accessed on 15 February 2024).
8. Chen, Z.; Lu, C. Humidity sensors: A review of materials and mechanisms. *Sens. Lett.* **2005**, *3*, 274–295. [CrossRef]
9. Montes-García, V.; Samorì, P. Humidity sensing with supramolecular nanostructures. *Adv. Mater.* **2024**, *36*, 2208766. [CrossRef] [PubMed]
10. Grundler, M.; Derieth, T.; Heinzel, A. Polymer compounds with high thermal conductivity. In *AIP Conference Proceedings*; AIP Publishing: College Park, MD, USA, 2016; Volume 1779.
11. Haq, Y.U.; Ullah, R.; Mazhar, S.; Khattak, R.; Qarni, A.A.; Haq, Z.U.; Amin, S. Synthesis and characterization of 2D MXene: Device fabrication for humidity sensing. *J. Sci. Adv. Mater. Devices* **2022**, *7*, 100390. [CrossRef]
12. Yasaei, P.; Behranginia, A.; Foroozan, T.; Asadi, M.; Kim, K.; Khalili-Araghi, F.; Salehi-Khojin, A. Stable and selective humidity sensing using stacked black phosphorus flakes. *ACS Nano* **2015**, *9*, 9898–9905. [CrossRef]
13. Emperhoff, S.; Eberl, M.; Dwertmann, T.; Wöllenstein, J. Humidity Impact on Thermal Conductivity Sensors. *Proceedings* **2024**, *97*, 93. [CrossRef]
14. Zheng, Z.; Zhang, G.; Wang, X.; Kong, X. Comparative Study of Gravimetric Humidity Sensor Platforms Based on CMUT and QCM. *Micromachines* **2022**, *13*, 1651. [CrossRef] [PubMed]
15. Rao, X.; Zhao, L.; Xu, L.; Wang, Y.; Liu, K.; Wang, Y.; Chen, G.Y.; Liu, T.; Wang, Y. Review of optical humidity sensors. *Sensors* **2021**, *21*, 8049. [CrossRef] [PubMed]
16. Le, X.; Liu, Y.; Peng, L.; Pang, J.; Xu, Z.; Gao, C.; Xie, J. Surface acoustic wave humidity sensors based on uniform and thickness controllable graphene oxide thin films formed by surface tension. *Microsyst. Nanoeng.* **2019**, *5*, 36. [CrossRef] [PubMed]
17. Yang, M.R.; Chen, K.S. Humidity sensors using polyvinyl alcohol mixed with electrolytes. *Sens. Actuators B Chem.* **1998**, *49*, 240–247. [CrossRef]
18. Tu, J.; Li, N.; Geng, W.; Wang, R.; Lai, X.; Cao, Y.; Qiu, S. Study on a type of mesoporous silica humidity sensing material. *Sens. Actuators B Chem.* **2012**, *166*, 658–664. [CrossRef]
19. Memon, M.M.; Hongyuan, Y.; Pan, S.; Wang, T.; Zhang, W. Surface Acoustic Wave Humidity Sensor Based on Hydrophobic Polymer Film. *J. Electron. Mater.* **2022**, *51*, 5627–5634. [CrossRef]
20. Dong, W.; Ma, Z.; Duan, Q. Preparation of stable crosslinked polyelectrolyte and the application for humidity sensing. *Sens. Actuators B Chem.* **2018**, *272*, 14–20. [CrossRef]
21. Rimeika, R.; Čiplys, D.; Poderys, V.; Rotomskis, R.; Balakauskas, S.; Shur, M.S. Subsecond-response S.A.W. humidity sensor with porphyrin nanostructure deposited on bare and metallised piezoelectric substrate. *Electron. Lett.* **2007**, *43*, 1055–1057. [CrossRef]
22. Monereo, O.; Claramunt, S.; de Marigorta, M.M.; Boix, M.; Leghrib, R.; Prades, J.; Cornet, A.; Merino, P.; Merino, C.; Cirera, A. Flexible sensor based on carbon nanofibers with multifunctional sensing features. *Talanta* **2013**, *107*, 239–247. [CrossRef]
23. Chu, J.; Peng, X.; Feng, P.; Sheng, Y.; Zhang, J. Study of humidity sensors based on nanostructured carbon films produced by physical vapor deposition. *Sens. Actuators B Chem.* **2013**, *178*, 508–513. [CrossRef]
24. Sharath Kumar, J.; Murmu, N.C.; Kuila, T. Recent Advances in Functionalized Micro and Mesoporous Carbon Nanostructures for Humidity Sensors. In *Functional Nanomaterials: Advances in Gas Sensing Technologies*; Spring: Berlin/Heidelberg, Germany, 2020; pp. 349–381.
25. Duan, Z.; Yuan, Z.; Jiang, Y.; Liu, Y.; Tai, H. Amorphous carbon material of daily carbon ink: Emerging applications in pressure, strain, and humidity sensors. *J. Mater. Chem. C* **2023**, *11*, 5585–5600. [CrossRef]
26. Rivadeneyra, A.; Salmeron, J.F.; Murru, F.; Lapresta-Fernández, A.; Rodríguez, N.; Capitan-Vallvey, L.F.; Salinas-Castillo, A. Carbon dots as sensing layer for printed humidity and temperature sensors. *Nanomaterials* **2020**, *10*, 2446. [CrossRef] [PubMed]
27. Frattini, G.; Torres, S.; Silva, L.I.; Repetto, C.E.; Gómez, B.; Dobry, A. The effect of nitriding on the humidity sensing properties of hydrogenated amorphous carbon films. *Phys. Scr.* **2021**, *96*, 055701. [CrossRef]
28. Yu, X.; Chen, X.; Yu, X.; Chen, X.; Ding, X.; Zhao, X. Flexible wearable humidity sensor based on nanodiamond with fast response. *IEEE Trans. Electron Devices* **2019**, *66*, 1911–1916. [CrossRef]
29. Wu, J.; Sun, Y.M.; Wu, Z.; Li, X.; Wang, N.; Tao, K.; Wang, G.P. Carbon nanocoil-based fast-response and flexible humidity sensor for multifunctional applications. *ACS Appl. Mater. Interfaces* **2019**, *11*, 4242–4251. [CrossRef]
30. Chen, W.P.; Zhao, Z.G.; Liu, X.W.; Zhang, Z.X.; Suo, C.G. A capacitive humidity sensor based on multi-wall carbon nanotubes (MWCNTs). *Sensors* **2009**, *9*, 7431–7444. [CrossRef]

31. Saxena, S.; Srivastava, A.K. Carbon nanotube-based sensors and their application. In *Nano-Optics*; Elsevier: Amsterdam, The Netherlands, 2020; pp. 265–291.

32. Tripathi, D.; Tripathi, S.; Rawat, R.K.; Chauhan, P. Highly Sensitive Humidity Sensor Based on Freestanding Graphene Oxide Sheets for Respiration and Moisture Detection. *J. Electron. Mater.* **2023**, *52*, 2396–2408. [CrossRef]

33. Lv, C.; Hu, C.; Luo, J.; Liu, S.; Qiao, Y.; Zhang, Z.; Song, J.; Shi, Y.; Cai, J.; Watanabe, A. Recent advances in graphene-based humidity sensors. *Nanomaterials* **2019**, *9*, 422. [CrossRef]

34. Liang, T.; Hou, W.; Ji, J.; Huang, Y. Wrinkled reduced graphene oxide humidity sensor with fast response/recovery and flexibility for respiratory monitoring. *Sens. Actuators A Phys.* **2023**, *350*, 114104. [CrossRef]

35. Wu, X.; Wu, H.; Jin, F.; Ge, H.L.; Gao, F.; Wu, Q.; Yang, H. Facile preparation of fullerenol-based humidity sensor with highly fast response. *Fuller. Nanotub. Carbon Nanostructures* **2023**, *31*, 1132–1136. [CrossRef]

36. Li, X.; Chen, X.; Yu, X.; Chen, X.; Ding, X.; Zhao, X. A high-sensitive humidity sensor based on water-soluble composite material of fullerene and graphene oxide. *IEEE Sens. J.* **2017**, *18*, 962–966. [CrossRef]

37. Selvam, K.P.; Nakagawa, T.; Marui, T.; Inoue, H.; Nishikawa, T.; Hayashi, Y. Synthesis of solvent-free conductive and flexible cellulose–carbon nanohorn sheets and their application as a water vapor sensor. *Mater. Res. Express* **2020**, *7*, 056402. [CrossRef]

38. Serban, B.C.; Buiu, O.; Dumbravescu, N.; Cobianu, C.; Avramescu, V.; Brezeanu, M.; Bumbac, M.; Pachiu, C.; Nicolescu, C.M. Oxidized carbon nanohorn-hydrophilic polymer nanocomposite as the resistive sensing layer for relative humidity. *Anal. Lett.* **2021**, *54*, 527–540. [CrossRef]

39. Serban, B.-C.; Cobianu, C.; Buiu, O.; Bumbac, M.; Dumbravescu, N.; Avramescu, V.; Nicolescu, C.M.; Brezeanu, M.; Pachiu, C.; Craciun, G.; et al. Ternary nanocomposites based on oxidized carbon nanohorns as sensing layers for room temperature resistive humidity sensing. *Materials* **2021**, *14*, 2705. [CrossRef]

40. Serban, B.C.; Cobianu, C.; Buiu, O.; Bumbac, M.; Dumbravescu, N.; Avramescu, V.; Nicolescu, C.M.; Brezeanu, M.; Radulescu, C.; Craciun, G.; et al. Quaternary Holey Carbon Nanohorns/SnO$_2$/ZnO/PVP Nano-Hybrid as Sensing Element for Resistive-Type Humidity Sensor. *Coatings* **2021**, *11*, 1307. [CrossRef]

41. Serban, B.C.; Buiu, O.; Bumbac, M.; Dumbravescu, N.; Avramescu, V.; Brezeanu, M.; Radulescu, C.; Craciun, G.; Nicolescu, C.M.; Romanitan, C.; et al. Ternary Holey Carbon Nanohorns/TiO$_2$/PVP Nanohybrids as Sensing Films for Resistive Humidity Sensors. *Coatings* **2021**, *11*, 1065. [CrossRef]

42. Song, X.; Qi, Q.; Zhang, T.; Wang, C. A humidity sensor based on KCl-doped SnO$_2$ nanofibers. *Sens. Actuators B Chem.* **2009**, *138*, 368–373. [CrossRef]

43. Qi, Q.; Zhang, T.; Wang, S.; Zheng, X. Humidity sensing properties of KCl-doped ZnO nanofibers with super-rapid response and recovery. *Sens. Actuators B Chem.* **2009**, *137*, 649–655. [CrossRef]

44. Geng, W.; Yuan, Q.; Jiang, X.; Tu, J.; Duan, L.; Gu, J.; Zhang, Q. Humidity sensing mechanism of mesoporous MgO/KCl–SiO$_2$ composites analyzed by complex impedance spectra and bode diagrams. *Sens. Actuators B Chem.* **2012**, *174*, 513–520. [CrossRef]

45. Kunchakara, S.; Dutt, M.; Ratan, A.; Shah, J.; Singh, V.; Kotnala, R.K. Synthesis and characterizations of highly ordered KCl–MCM–41 porous nanocomposites for impedimetric humidity sensing. *J. Porous Mater.* **2019**, *26*, 389–398. [CrossRef]

46. Wang, W.; Li, Z.; Liu, L.; Zhang, H.; Zheng, W.; Wang, Y.; Wang, C. Humidity sensor based on LiCl-doped ZnO electrospun nanofibers. *Sens. Actuators B Chem.* **2009**, *141*, 404–409. [CrossRef]

47. Buvailo, A.I.; Xing, Y.; Hines, J.; Dollahon, N.; Borguet, E. TiO$_2$/LiCl-based nanostructured thin film for humidity sensor applications. *ACS Appl. Mater. Interfaces* **2011**, *3*, 528–533. [CrossRef] [PubMed]

48. Jiang, Y.; Duan, Z.; Fan, Z.; Yao, P.; Yuan, Z.; Jiang, Y.; Tai, H. Power generation humidity sensor based on NaCl/halloysite nanotubes for respiratory patterns monitoring. *Sens. Actuators B Chem.* **2023**, *380*, 133396. [CrossRef]

49. Lazarus, N.; Bedair, S.S.; Lo, C.C.; Fedder, G.K. CMOS-MEMS capacitive humidity sensor. *J. Microelectromech. Syst.* **2009**, *19*, 183–191. [CrossRef]

50. Muto, S.; Suzuki, O.; Amano, T.; Morisawa, M. A plastic optical fiber sensor for real-time humidity monitoring. *Meas. Sci. Technol.* **2003**, *14*, 746. [CrossRef]

51. Penza, M.; Anisimkin, V.I. Surface acoustic wave humidity sensor using polyvinyl-alcohol film. *Sens. Actuators A* **1999**, *76*, 162–166. [CrossRef]

52. Su, P.G.; Wang, C.S. Novel flexible resistive-type humidity sensor. *Sens. Actuators B Chem.* **2007**, *123*, 1071–1076. [CrossRef]

53. Zhang, M.; Duan, Z.; Zhang, B.; Yuan, Z.; Zhao, Q.; Jiang, Y.; Tai, H. Electrochemical humidity sensor enabled self-powered wireless humidity detection system. *Nano Energy* **2023**, *115*, 108745. [CrossRef]

54. Arman Kuzubasoglu, B. Recent studies on the humidity sensor: A mini review. *ACS Appl. Electron. Mater.* **2022**, *4*, 4797–4807. [CrossRef]

55. Shooshtari, M.; Salehi, A.; Vollebregt, S. Effect of humidity on gas sensing performance of carbon nanotube gas sensors operated at room temperature. *IEEE Sens. J.* **2020**, *21*, 5763–5770. [CrossRef]

56. Serban, B.-C.; Cobianu, C.; Buiu, O.; Bumbac, M.; Dumbravescu, N.; Avramescu, V.; Nicolescu, C.M.; Brezeanu, M.; Radulescu, C.; Craciun, G.; et al. Quaternary Oxidized Carbon Nanohorns—Based Nanohybrid as Sensing Coating for Room Temperature Resistive Humidity Monitoring. *Coatings* **2021**, *11*, 530. [CrossRef]

57. Heidari, B.; Salmani, S.; Sasani Ghamsari, M.; Ahmadi, M.; Majles-Ara, M.H. Ag/PVP nanocomposite thin film with giant optical nonlinearity. *Opt. Quantum Electron.* **2020**, *52*, 86. [CrossRef]

58. Le, G.T.; Lerkprasertkun, P.; Sano, N.; Wu KC, W.; Charinpanitkul, T. Carbon nanohorns with surface functionalized by plasma treatment and their applications in drug delivery systems. *J. Sci. Adv. Mater. Devices* **2023**, *8*, 100616. [CrossRef]

59. Santra, S.; Hu, G.; Howe, R.C.T.; De Luca, A.; Ali, S.Z.; Udrea, F.; Gardner, J.W.; Ray, S.K.; Guha, P.K.; Hasan, T. CMOS integration of inkjet-printed graphene for humidity sensing. *Sci. Rep.* **2015**, *5*, 17374. [CrossRef] [PubMed]

60. Borini, S.; White, R.; Wei, D.; Astley, M.; Haque, S.; Spigone, E.; Harris, N.; Kivioja, J.; Ryhanen, T. Ultrafast graphene oxide humidity sensors. *ACS Nano* **2013**, *7*, 11166–11173. [CrossRef]

61. Li, B.; Weng, X.; Sun, X.; Zhang, Y.; Lv, X.; Gu, G. Facile synthesis of Fe_3O_4/reduced graphene oxide/polyvinyl pyrrolidone ternary composites and their enhanced microwave absorbing properties. *J. Saudi Chem. Soc.* **2018**, *22*, 979–984. [CrossRef]

62. Serban, B.-C.; Cobianu, C.; Dumbravescu, N.; Buiu, O.; Bumbac, M.; Nicolescu, C.M.; Cobianu, C.; Brezeanu, M.; Pachiu, C.; Serbanescu, M. Electrical percolation threshold and size effects in polyvinylpyrrolidone-oxidized single-wall carbon nanohorn nanocomposite: The impact for relative humidity resistive sensors design. *Sensors* **2021**, *21*, 1435. [CrossRef]

63. Serban, B.C.; Cobianu, C.; Dumbravescu, N.; Buiu, O.; Avramescu, V.; Bumbac, M.; Nicolescu, C.M.; Cobianu, C.; Brezeanu, M. Electrical percolation threshold in oxidized single wall carbon nanohorn-polyvinylpyrrolidone nanocomposite: A possible application for high sensitivity resistive humidity sensor. In Proceedings of the 2020 International Semiconductor Conference (CAS), Sinaia, Romania, 7–9 October 2020; IEEE: Piscataway Township, NJ, USA, 2020; pp. 239–242.

64. Serban, B.; Kumar, A.S.; Cobianu, C.; Buiu, O.; Costea, S.; Bostan, C.; Varachiu, N. Selection of gas sensing materials using the Hard Soft Acid Base theory; application to Surface Acoustic Wave CO_2 detection. In Proceedings of the CAS 2010 Proceedings (International Semiconductor Conference), Sinaia, Romania, 11–13 October 2010; IEEE: Piscataway Township, NJ, USA, 2010; Volume 1, pp. 247–250.

65. Serban, B.C.; Brezeanu, M.; Cobianu, C.; Costea, S.; Buiu, O.; Stratulat, A.; Varachiu, N. Materials selection for gas sensing. An HSAB perspective. In Proceedings of the 2014 International Semiconductor Conference (CAS), Sinaia, Romania, 13–15 October 2014; IEEE: Piscataway Township, NJ, USA, 2014; pp. 21–30.